

Active Diffusion of Self-Propelled Particles in Semi-Flexible Polymer Networks

Yeongjin Kim,¹ Won Kyu Kim,^{2,*} and Jae-Hyung Jeon^{1,3,†}

¹*Department of Physics, Pohang University of Science and Technology (POSTECH), Pohang 37673, Republic of Korea*

²*School of Computational Sciences, Korea Institute for Advanced Study (KIAS), Seoul 02455, Republic of Korea*

³*Asia Pacific Center for Theoretical Physics (APCTP), Pohang 37673, Republic of Korea*

Mesh-like structures, such as mucus gel or cytoskeleton networks, are ubiquitous in biological systems. These intricate structures are composed of cross-linked, semi-flexible bio-filaments, crucial to numerous biological processes. In many biological systems, active self-propelled particles like motor proteins or bacteria navigate these intricate polymer networks. In this study, we develop a computational model of three-dimensional cubic-topological, swollen polymer networks of semi-flexible filaments. We perform Langevin dynamics simulations to investigate the diffusion of active tracer particles navigating through these networks. By analyzing various physical observables, we investigate the effects of mesh-to-particle size ratio, Péclet number of active particles, and bending stiffness of the polymer networks upon active trapped-and-hopping diffusion of the tracer. When the tracer size is equal to or larger than the mesh size, the polymer stiffness substantially enhances trapping while suppressing the hopping process. Notably, the mean trapped time exhibits an exponential growth law to the bending stiffness with an activity-dependent slope. An analytic theory based on the mean first-passage time of active particles in a harmonic potential is developed. Our findings deepen the comprehension of the intricate interplay between the polymer's bending stiffness, tracer size, and the activity of tracer particles. This knowledge can shed light on important biological processes, such as motor-driven cargo transport or drug delivery, which hinge on the behavior of active particles within biological gels.

I. INTRODUCTION

Biopolymer networks of semi-flexible filaments having a large bending persistent length are ubiquitous in biological cells, such as collagen, actin, microtubules, and DNA networks [1]. In many biosystems, the flexural stiffness of biopolymers is a critical physical component that significantly influences various biological properties. For instance, the stiffness of the cellular environment determines the morphing of a stem cell [2]. Moreover, semi-flexibility plays a vital role in biopolymer network topology and cosolute partitioning [3]. The stiffness of the mucus layer is important in its physiological functions where the mucus has the ability to restore its initial stiffness through biological processes [4]. It is also known that the stiffness of the extracellular matrix plays a vital role in tumor cell migration [5].

Living systems are highly dynamic and active, as they utilize components that convert chemical energies (e.g., ATPs) from the environment into mechanical ones, driving the system out of equilibrium. The entities converting the energies to motion can be regarded as active or self-propelled particles [6–8]. Prominent examples include motor proteins such as kinesin and dynein and microswimmers like *E. coli* bacteria [9–12]. The nonequilibrium diffusion dynamics of various active particles have been extensively explored both experimentally and theoretically [13, 14]. Beyond the single-particle dynamics, quantitative understanding of the active particles in geometric or potential confinement, polymeric environments, and other complex environments is a currently keen interest [8, 11, 15–36].

The thermal diffusion of Brownian tracers in a polymer network has been extensively investigated. These studies reveal that various diffusion dynamics can emerge depending on the physical conditions of mesh-to-particle size ratio, topology and stiffness of the network, and interactions between the polymer and particles [37–51]. In contrast, the dynamics of active tracers in polymer networks remain relatively unexplored. Limited attempts have investigated the diffusion of active particles, primarily in polymer solutions or melts [18, 19, 52–57], or within random matrices [23, 25, 35]. Addressing this research gap, we recently introduced a computational model of active tracer particles in a flexible cubic polymer network. Through explicit simulations, we examined the diffusion of active tracers navigating this flexible polymer environment [58]. It turned out that geometrically trapped mesh-sized tracers can freely diffuse in the polymer network via the activeness-induced hopping mechanism. The trapped times obey an exponential law, with the mean trapped time decreasing with increased activeness (quantified with Péclet number). Furthermore, active tracers always reach the regime of Fickian diffusion in the long-time limit in which the diffusivity increases with the Péclet number with three distinct scaling regimes.

Beyond our previous computational study, in this work, we focus on the active diffusion of self-propelled particles in a *semi-flexible* polymer network. We explicitly model a semi-flexible polymer network of cubic topology with various bending stiffness, simulating the diffusion of mesh-sized active particles (i.e., active Ornstein-Uhlenbeck particles and active Brownian particles) therein. We find that in semi-flexible networks, the characteristics of active diffusion are critically determined by the geometrical factor including the mesh-to-particle size ratio. We quantify how the bending stiffness impacts the characteristics of trapped and hopping dynamics of active tracers in terms of various phys-

* wonkyukim@kias.re.kr

† jeonjh@postech.ac.kr

ical observables. While the flight length mildly decreases with the bending stiffness, the trapped time exponentially increases with it. We also present an active barrier-crossing theory to quantitatively account for the observed exponential growth law of the trapped time against the bending stiffness. Our computational and analytic studies altogether demonstrate a significant role of the semi-flexibility of the polymer network in the active transport of tracers.

The current work is structured as follows. In Sec. II, we introduce the simulated semi-flexible polymer network system and also explain the model of active tracers and the physical observables under examination. In Sec. III, we present our simulation and analytic results. For three distinct tracer sizes, we investigate the properties of their respective active diffusion in Secs. III A–III C. Then, we present a first-passage barrier-crossing theory of an active Ornstein-Uhlenbeck particle confined to a harmonic potential in Sec. III D. We encapsulate and discuss the main results in Sec. IV, along with the additional simulation result for active Brownian particles. Finally, conclusions are provided in Sec. V.

II. MODEL AND METHODS

A. The polymer network

We construct a cubic network of semi-flexible polymers in three dimensions (Fig. 1a), representing swollen polymer gels that we are interested in. The monomers comprising the polymer network are identical with size of σ_0 and the polymer consists of four monomers, which are interconnected between the nearest cross-linkers. The monomers are subject to the bonding potential U_{bond} and the bending potential U_{bend} . For the bonding potential, we use a bead-spring model, $U_{\text{bond}}(r) = k_b(r - l_b)^2$, where $k_b = 100 k_B T / \sigma_0^2$ is the spring constant [59], and $l_b = \sigma_0$ is the bond length. For the bending potential, we adopt a harmonic potential $U_{\text{bend}}(\theta) = \kappa(\theta - \pi)^2$, where θ is the angle between two bonds, and κ is the bending stiffness (modulus) of the polymer network. The stiffness parameter κ can be converted into the persistence length (l_p) of a semi-flexible polymer via [3]

$$l_p = \frac{2\kappa\sigma_0}{k_B T}. \quad (1)$$

Figure 1a illustrates a semi-flexible polymer network ($\kappa = 40 k_B T$) and the polymer bending conformations are compared with those with different bending stiffness ($\kappa = 0, 10 k_B T$, and $100 k_B T$). It shows that larger stiffness suppresses the fluctuations of the polymer network in the transverse direction, rendering the network more rigid. In the presence of large fluctuations of the polymer network, the tracer particles therein (red spheres in Fig. 1a) experience a significant amount of excluded volume, thereby reducing the accessible volume of the tracers within a mesh. Figure S1 in the Supplementary Material presents the bond-

length and angle distributions of the polymer networks for varying κ .

B. The active tracers and governing equations

We consider the so-called Active Ornstein-Uhlenbeck (AOU) processes, in which a self-propelled, AOUP particle (AOUP) of mass m is fueled by an active force \mathbf{F}_A in the Langevin dynamics,

$$\frac{d\mathbf{r}}{dt} = \mathbf{v}, \quad m \frac{d\mathbf{v}}{dt} = -\gamma\mathbf{v} + \mathbf{F}_A + \boldsymbol{\xi}. \quad (2)$$

Here, $\mathbf{r}(t)$ is the three-dimensional position, $\mathbf{v}(t)$ is the velocity, γ is the friction coefficient, and $\boldsymbol{\xi} = (\xi^x, \xi^y, \xi^z)$ is the thermal white noise with $\langle \xi^\alpha \rangle = 0$ and $\langle \xi^\alpha(t) \xi^\beta(t') \rangle = 2\gamma k_B T \delta_{\alpha\beta} \delta(t - t')$ where α, β denote the Cartesian components.

The active force, \mathbf{F}_A , is the OU process: stochastic and governed by the following equation of motion,

$$\frac{d\mathbf{F}_A}{dt} = -\frac{1}{\tau_A} \mathbf{F}_A + \sqrt{\frac{2\gamma^2 v_p^2}{3\tau_A}} \boldsymbol{\xi}_A(t), \quad (3)$$

where $\boldsymbol{\xi}_A = (\xi_A^x, \xi_A^y, \xi_A^z)$ satisfies $\langle \boldsymbol{\xi}_A \rangle = \mathbf{0}$ and $\langle \xi_A^\alpha(t) \xi_A^\beta(t') \rangle = \delta_{\alpha\beta} \delta(t - t')$, yielding an exponentially decaying correlation in time,

$$\langle F_A^\alpha(t) F_A^\beta(t') \rangle = \frac{\gamma^2 v_p^2}{3} \delta_{\alpha\beta} e^{-|t-t'|/\tau_A}. \quad (4)$$

Here, v_p represents the strength of propulsion velocity, and τ_A represents the directional persistent time. This enables us to define the persistence length of AOUP's trajectory as $R_p = v_p \tau_A$ [60, 61].

From Eqs. (2)–(4), the mean-square displacement of AOUP is derived as [60]

$$\begin{aligned} \langle \Delta \mathbf{r}^2(t) \rangle_{\text{free}} &= 6D_{\text{th}}(t - \tau_0(1 - e^{-t/\tau_0})) \\ &+ 2v_p^2 \tau_A \left[\frac{t - \tau_A(1 - e^{-t/\tau_A})}{1 - \tau_0^2/\tau_A^2} - \frac{\tau_0^2}{\tau_A^2} \frac{t - \tau_0(1 - e^{-t/\tau_0})}{1 - \tau_0^2/\tau_A^2} \right], \end{aligned} \quad (5)$$

where, $D_{\text{th}} = k_B T / \gamma$ is the long-time diffusivity of a passive Brownian particle, and $\tau_0 = m / \gamma$ is the momentum relaxation time.

A quantity of importance representing a degree of activity of AOUPs is the Péclet number (Pe), which is defined by

$$\text{Pe} = \frac{\sigma_{\text{tr}} v_p}{D_{\text{th}}} = \frac{3\pi\eta\sigma_{\text{tr}}^2 v_p}{k_B T} \quad (6)$$

where σ_{tr} is the AOUP's size (diameter) and η is the viscosity of the medium, which satisfies the Stokes law, $\gamma = 3\pi\eta\sigma_{\text{tr}}$.

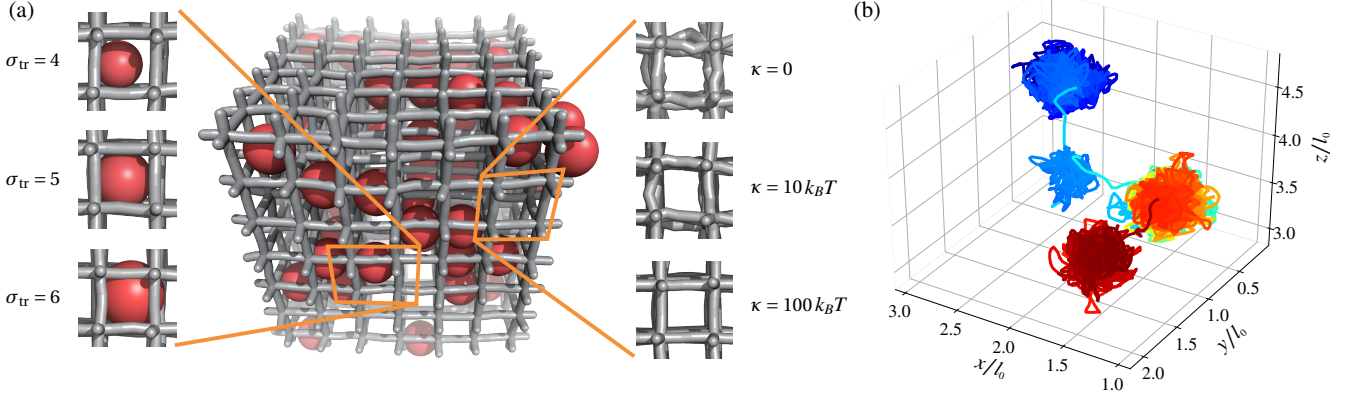


FIG. 1. (a) Active tracers (red) in a semi-flexible polymer network gel (gray). The left side illustrates active tracers of varying sizes ($\sigma_{\text{tr}} = 4, 5, \text{ and } 6$). On the right side, representative configurations of flexible and semi-flexible polymer networks with different bending stiffnesses ($\kappa = 0, 10 k_B T, \text{ and } 100 k_B T$) are shown. (b) Representative 'trapped-and-hopping' trajectory of a mesh-sized active tracer in the semi-flexible polymer network. The color code depicts the elapsed time (from yellow to blue). We use the tracer diameter $\sigma_{\text{tr}} = 5$, the Péclet number $\text{Pe} = 18$, and the stiffness $\kappa = 40 k_B T$.

C. Non-boned interactions and simulations

We employ the Lennard–Jones potential for the non-bonded interactions between particles i and j ,

$$U_{\text{LJ}}^{ij}(r_{ij}) = \begin{cases} 4\epsilon_{ij} \left[\left(\frac{\sigma_{ij}}{r_{ij}} \right)^{12} - \left(\frac{\sigma_{ij}}{r_{ij}} \right)^6 \right] - U_c & , r_{ij} \leq r_c \\ 0 & , r_{ij} > r_c. \end{cases} \quad (7)$$

Here, r_{ij} is the distance between two particles and $\sigma_{ij} = \frac{1}{2}(\sigma_{ii} + \sigma_{jj})$, $r_c = 2.5\sigma_{ij}$ is the cut-off length, and $U_c = 4\epsilon_{ij} \left[\frac{1}{2.5^{12}} - \frac{1}{2.5^6} \right]$. We use $\epsilon_{\text{m m}} = \epsilon_{\text{m c}} = \epsilon_{\text{c c}} = \epsilon_{\text{m tr}} = \epsilon_{\text{c tr}} = 0.1 k_B T$, which represents the repulsive interactions (excluded volumes) between the monomers (m), cross-linkers (c), and tracers (tr) [62]. For an infinitely dilute condition, we use $\epsilon_{\text{tr tr}} = 0$, similarly to our previous study [58].

We run Langevin dynamics simulations incorporating the system setup and interactions described above. The equation of motion of i -th monomer is

$$\frac{d\mathbf{r}_i}{dt} = \mathbf{v}_i, \quad m \frac{d\mathbf{v}_i}{dt} = -\gamma_i \mathbf{v}_i - \nabla_i U_m + \boldsymbol{\xi}_i. \quad (8)$$

Here, $-\nabla_i U_m$ is the force acting on the i -th monomer, where the total potential is $U_m = \sum_{ij} [U_{\text{bond}}(r_{ij}) + U_{\text{LJ}}(r_{ij})] + \sum_{\theta} U_{\text{angle}}(\theta)$, and $\gamma_i = 3\pi\eta\sigma_i$ is the friction coefficient.

For the k -th AOPUs as tracers, the equation of motion is

$$\frac{d\mathbf{r}_k}{dt} = \mathbf{v}_k, \quad m \frac{d\mathbf{v}_k}{dt} = -\gamma_k \mathbf{v}_k - \nabla_k U + \mathbf{F}_{\text{A},k} + \boldsymbol{\xi}_k, \quad (9)$$

where $U = \sum_{ij} [U_{\text{LJ}}(r_{ij})]$ is the tracer's total LJ potential.

The stochastic active force $\mathbf{F}_{\text{A},k}(t)$ is generated based on Eq. (3) for each tracer of index k , for which we consider 100 tracers and $\tau_{\text{A}} = 10$. We use the LAMMPS simulation package [63] to run the above coupled equations of motions with the self-written input scripts. We use the LJ unit, which sets

the unit length σ_0 and unit time $t_0 = \sqrt{m\sigma_0^2/k_B T}$. The simulation box is of size $35 \times 35 \times 35$ and periodic, in which seven cross-linkers exist per one linear polymer (total $7 \times 7 \times 7$ cross-linkers). We use the time step $\delta t = 0.001$ and the total run time is typically $T = 5 \times 10^7 \delta t$.

D. Mean-square displacement, non-Gaussian parameter, trapped times, and flight lengths

From the relative particle position at time t , $\mathbf{r}_{\text{rel},i}(t) = \mathbf{r}_i(t) - \mathbf{r}_{\text{cm}}(t)$, where $\mathbf{r}_i(t)$ is the i -th particle's position and $\mathbf{r}_{\text{cm}}(t)$ is the center-of-mass position of the system, we quantify the characteristic of trapped-and-hopping dynamics by measuring the mean-square displacement (MSD), non-Gaussian parameter (NGP), trapped time (τ), and flight length (l).

We define MSD as

$$\langle \Delta \mathbf{r}_{\text{rel}}^2(t) \rangle = \frac{1}{N} \sum_i \frac{1}{T-t} \int_0^{T-t} (\mathbf{r}_{\text{rel},i}(t'+t) - \mathbf{r}_{\text{rel},i}(t'))^2 dt', \quad (10)$$

where N denotes the number of tracers ($N = 100$).

From the MSD data, we select a time interval, in which $t > 20$ and the MSD exponent $\alpha = \frac{d \log \langle \mathbf{r}_{\text{rel}}^2(t) \rangle}{d \log t}$ falls within the range $0.95 < \alpha(t) < 1.05$. We then fit the MSD via $\langle \mathbf{r}_{\text{rel}}^2(t) \rangle = 6D_L t$, where long-time diffusivity (D_L) is the fitting parameter.

We define NGP(t) from the relative position $\mathbf{r}_{\text{rel},i}(t)$, such that NGP in one dimension is

$$\text{NGP}(t) = \frac{\langle \Delta x^4(t) \rangle}{3 \langle \Delta x^2(t) \rangle^2} - 1, \quad (11)$$

where x is one of the Cartesian components for the relative position, t is the time lag, and the bracket $\langle \cdot \rangle$ represents both time and ensemble average [58].

We employ a bilateral filter to skeletonize obtained trajectories [58, 64] and collect trapped states and hopping states. Based on this, we calculate average trapped times and flight lengths.

III. RESULTS

From the simulations, we observe that small tracers (either passive or active) of size $\sigma_{\text{tr}} \approx 1$ diffuse inside the polymer network relatively freely. The polymer network acts as a trivial obstacle, thus the tracers' diffusion is suppressed by the percolated geometry, which is qualitatively similar to the free diffusion with decreased mobility [58] (Fig. A1).

However, we observe different diffusion dynamics when the tracer size becomes comparable to the mesh size of the network ($l_0 \approx 5$), featuring the trapped-and-hopping mechanism [58]. For instance, Fig. 1b shows a typical trapped-and-hopping trajectory of a mesh-sized ($\sigma_{\text{tr}} = 5$) AOUP tracer (of $\text{Pe} = 18$) in a semi-flexible polymer network ($\kappa = 40 k_B T$).

Our main interest lies in the effects of polymer semi-flexibility on such trapped-and-hopping diffusion dynamics of AOUPs. In the following, we consider three different AOUP tracer sizes: $\sigma_{\text{tr}} = 4$, $\sigma_{\text{tr}} = 5$, and $\sigma_{\text{tr}} = 6$ (Fig. 1a). We vary Pe in the range of 0–54 for $\sigma_{\text{tr}} = 4$, 0–90 for $\sigma_{\text{tr}} = 5$, and 0–180 for $\sigma_{\text{tr}} = 6$, respectively.

A. AOUPs with $\sigma_{\text{tr}} = 4$

First, we examine the case in which the tracer size is marginally smaller than the mesh size of the polymer network, i.e., $\sigma_{\text{tr}} = 4 \lesssim l_0 = 5$. Figure 2a shows $x(t)$ of the tracer in a flexible polymer network ($\kappa = 0$). Depending on Pe , the trajectory shows the occasional hopping dynamics, the distance of which increases with larger Pe . Such tendencies are still observed even for semi-flexible networks of $\kappa > 0$, i.e., the hopping dynamics is nearly independent of κ (data not shown).

Figure 2b shows the tracers' $\text{MSD}(t)$ for different Pe and κ . We find that the diffusion dynamics is almost independent of κ (different symbols with the same color), implying that the AOUP of $\sigma_{\text{tr}} = 4$ is still small and its hopping is subject to minimal contacts with the polymers. The red symbols depict the MSD of passive tracers ($\text{Pe} = 0$), showing the ballistic short-time regime ($\text{MSD} \sim t^2$) before reaching the momentum relaxation time ($t \lesssim \tau_0 = 1.2$), and the long-time hopping dynamics ($t \gtrsim \langle \tau \rangle \approx 50$) that is Fickian ($\text{MSD} \sim t^1$). Here, $\langle \tau \rangle$ is the mean trapped time. In the intermediate time ($\tau_0 \lesssim t \lesssim \langle \tau \rangle$), the exponent α of $\text{MSD}(t) \sim t^\alpha$ becomes smaller than unity, signifying the caging effect before reaching the normal diffusion ($\alpha = 1$). The blue symbols represent the MSD of active tracers with $\text{Pe} = 7$, showing the almost immediate crossover from the ballistic to Fickian dynamics without any significant intermediate subdiffusive time domain. This reflects that in the trapped state during the time in the range of $\tau_0 (\approx 1) \lesssim t \lesssim \langle \tau \rangle (\approx 15)$, the

active force (increasing α) and the trapping force (decreasing α) become comparable and compete with each other, resulting in the exponent α close to unity. When the activeness increases ($\text{Pe} = 18$), as shown by the green symbols, the activated hopping dynamics dominates, yielding the trapped time very short ($\langle \tau \rangle \approx 5$). The resultant MSD reveals three temporal regimes divided by the momentum relaxation time ($\tau_0 \approx 1$) and the directional persistent time ($\tau_A = 10$). In the short-time regime ($t \lesssim \tau_0$), similarly to the previous cases, the tracers undergo the ballistic dynamics featuring $\alpha = 2$. In the intermediate time ($\tau_0 \lesssim t \lesssim \tau_A$), however, the competition between the activeness and trapping force yields $\alpha \approx 1.5$. In the long-time regime, the MSD exhibits the Fickian dynamics with $\alpha = 1$ eventually.

Figure 2c depicts the NGP of the tracers with $\text{Pe} = 7$. The NGP is maximized at the timescale that the tracer starts to encounter the polymer networks as obstacles. Similarly to the MSD, we find that the overall behavior of NGPs barely depends on the polymer network's stiffness. However, the magnitude of the peaks slightly varies depending on κ , increasing with κ for the semi-flexible polymers. This effect is more dramatic for larger tracers, which we discuss further in the following sections.

Figures 2d, 2e, and 2f show the mean trapped time, the mean flight length, and the long-time diffusivity, as a function of κ , respectively. (The distributions of the trapped times and flight lengths are present in Figs. S2 and S3). Those key quantities of our interest are not significantly dependent on the polymer stiffness, in line with the tendency we find from $x(t)$ and MSD.

B. AOUPs with $\sigma_{\text{tr}} = 5$

Now we consider AOUPs whose size is equal to polymer network's mesh size ($\sigma_{\text{tr}} = l_0 = 5$). For a limiting reference, we also consider a network comprising rigid rod-like polymers ($\kappa \rightarrow \infty$), the conformational fluctuation of which vanishes.

Figure 3a shows MSDs of passive tracers ($\text{Pe} = 0$) for different κ . As similarly found in the previous section, we find that the MSD in the short-time ballistic regime ($t \lesssim \tau_0$) varies less sensitively with κ . The subsequent time regime exhibits the pronounced caged dynamics in $\tau_0 \lesssim t \lesssim \langle \tau \rangle$, after which the long-time Fickian dynamics reflects the hopping dynamics between network meshes.

The upper inset in Fig. 3a highlights two intriguing features of the short-time dynamics. One is the enhancement of MSD with increasing κ at very short time ($t \lesssim 1$). The conformational fluctuation of the flexible polymer network is larger than that of the semi-flexible polymer networks. This implies that the effective free volume accessible to the tracers is larger for stiffer networks. Therefore, the polymer networks with larger κ enhance the magnitudes of short-time MSDs. The other notable feature is the bounce-back dynamics, i.e., the oscillatory behavior of MSDs. This occurs when AOUPs bounce back and forth within a network mesh. We find that the bounce-back dy-

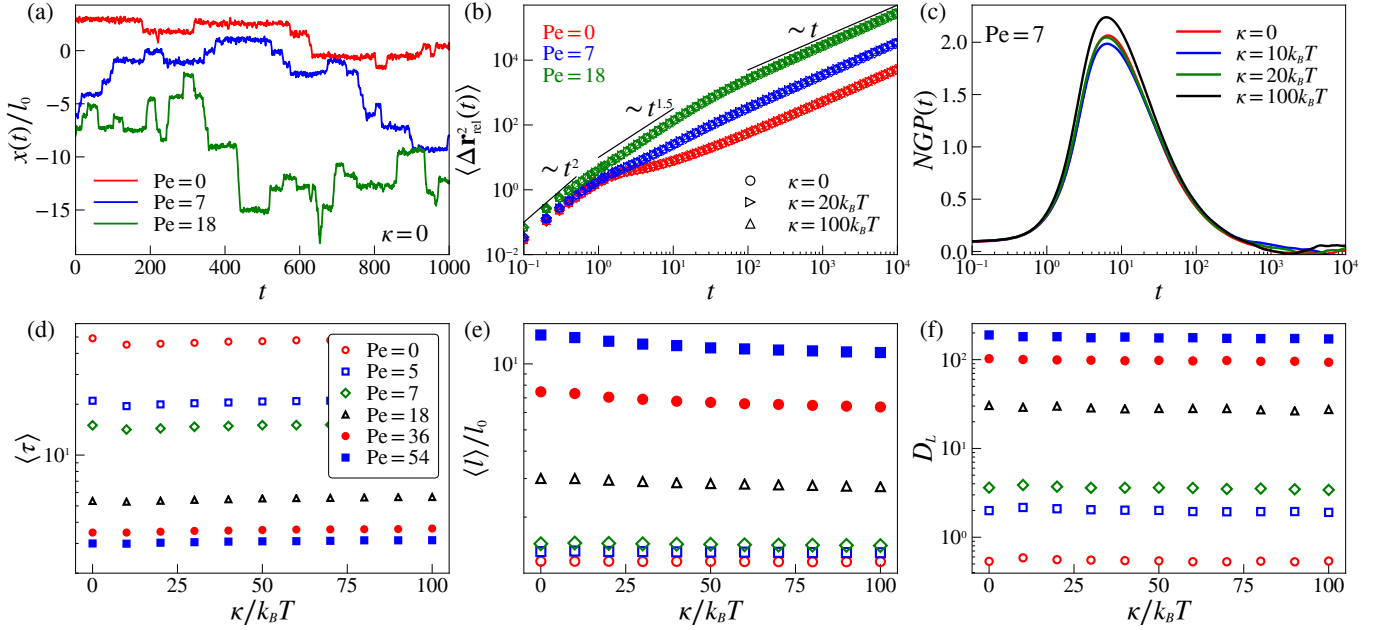


FIG. 2. (a) Time-dependent position $x(t)$ of an active tracer of size $\sigma_{\text{tr}} = 4$ in a flexible ($\kappa = 0$) polymer network, for different $\text{Pe} = 0, 7$, and 18 . (b) Mean-square displacement (MSD) of active tracers in polymer networks for different Pe and κ . (c) non-Gaussian parameter (NGP) of active tracers with $\text{Pe} = 7$ in polymer networks for different κ . (d) Mean trapped time $\langle \tau \rangle$, (e) mean flight length $\langle l \rangle$, and (f) long-time diffusivity D_L of active tracers as a function of κ for different Pe .

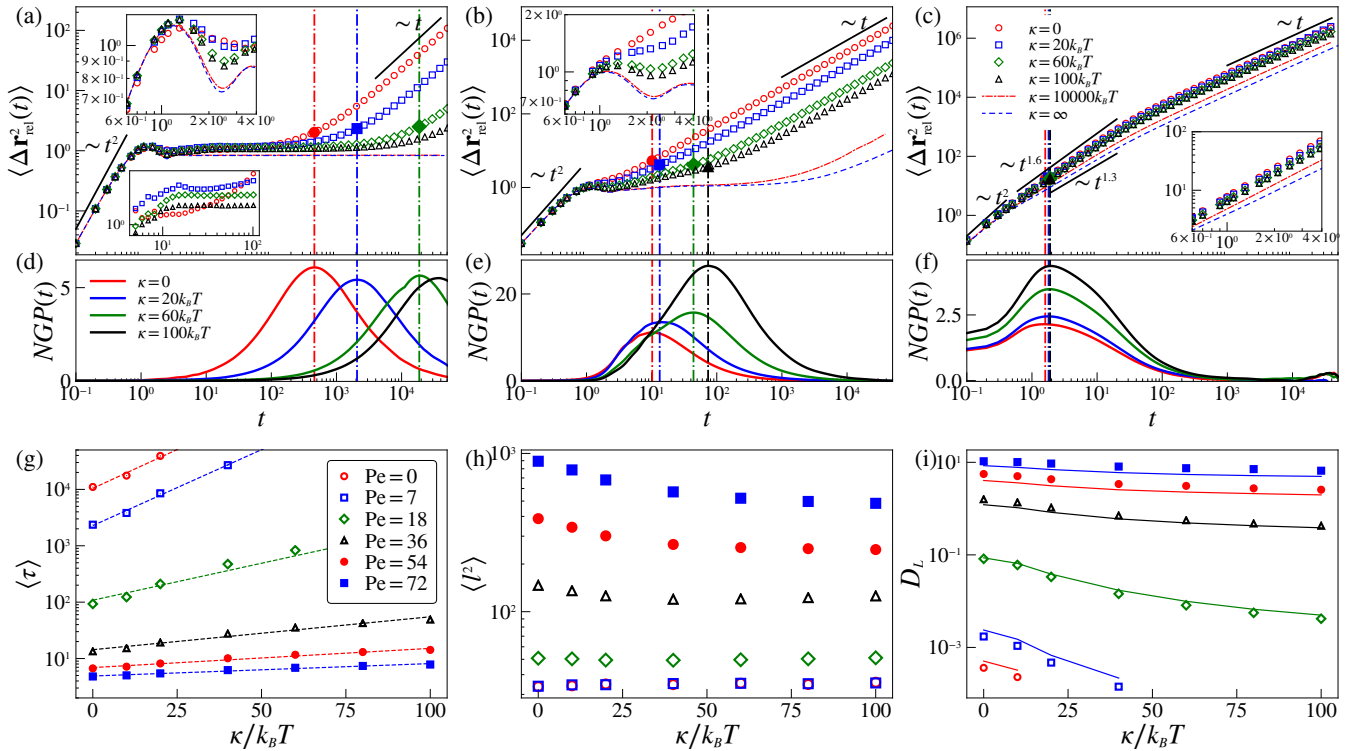


FIG. 3. MSD of tracers of size $\sigma_{\text{tr}} = 5$ for (a) $\text{Pe} = 0$, (b) $\text{Pe} = 18$, and (c) $\text{Pe} = 72$. NGP for (d) $\text{Pe} = 0$, (e) $\text{Pe} = 18$, and (f) $\text{Pe} = 72$. (g) Mean trapped time $\langle \tau \rangle$, (h) mean-square flight length $\langle l^2 \rangle$, and (i) long-time diffusivity D_L , as a function of κ , respectively. Solid lines in (i) depict D_L in Eq. (12).

namics originates from the underdamped dynamics under confinement, consistent with literature [65, 66]. For the same polymer network system, the overdamped AOUP does not exhibit the bounce-back dynamics (See our supplementary overdamped Langevin dynamics simulation in Fig. S4). For large κ , the bounce-back dynamics becomes more pronounced, yielding large oscillatory MSDs.

This tendency changes in the subsequent confined dynamics (see the lower inset in Fig. 3a). For semi-flexible networks of stiffness up to $\kappa = 20 k_B T$, the accessible free volume increases and the MSDs become larger. But for stiffer networks ($\kappa > 20 k_B T$), the shape of the potential of mean force, whose energy barrier is larger than the one of a flexible network ($\kappa = 0$), comes into a major play, resulting in decreasing MSDs with κ (see Fig. A2a for the potential of mean force).

When the activeness of AOUPs is larger ($Pe = 18$), as shown in the inset of Fig. 3b, we find that the bounce-back dynamics disappear for $\kappa < \kappa^* \approx 20 k_B T$, implying that the critical stiffness $\kappa^*(Pe)$ exists, above which the bounce-back dynamics occurs. In addition, as shown in Fig. 3b, the short-time dynamics ($t < 1$) barely depends on κ and the activated tracers undergo the later escape dynamics easily, resulting in the shortened intermediate confined dynamics.

When Pe is very large ($Pe = 72$), as shown in Fig. 3c, the active force dominates over the trapping force and we observe the similar tendency of MSD ($\alpha > 1$) found in Fig. 2b. There occurs a crossover between the superdiffusive, intermediate, and Fickian dynamics, divided by the momentum relaxation time τ_0 and the directional persistent time τ_A , in which the exponent value varies ($\alpha = 1.3-1.6$) in the intermediate time. Nevertheless, unlike in the small AOUPs' case, the MSD largely depends on κ and its magnitude decreases with κ .

Below the MSDs, in Figs. 3d-f, we show NGPs in the same time axes. We find that the NGPs have a peak (maximally non-Gaussian) at a certain intermediate time. The vertical lines depict this peak time of NGP, respectively, for different κ , and the solid symbols depict the corresponding MSDs at the peak time. What we first find is that the peak time of NGP increases as κ increases. However, the peak time becomes shorter and less dependent on κ for large Pe (see Figs. 3e and 3f). Although the peak time of NGP tends to be almost independent of κ for large Pe , the magnitude of peak increases with κ , unlike NGP for the case of $Pe = 0$. This means that the non-Gaussian dynamics is dictated by the high competition between the activeness and the trapping force enhanced by increasing κ , the mechanism of which is well captured by Fig. 3e at $Pe = 18$ where NGP's magnitude is around five times larger than the other cases (trapping dominant at $Pe = 0$ and activeness dominant at $Pe = 72$). This feature is also captured by the van-Hove self-correlation functions [58] (Fig. S5).

The trapped-and-hopping dynamics is also characterized by the mean trapped time $\langle \tau \rangle$ and the mean-square flight length $\langle l^2 \rangle$. Figure 3g shows $\langle \tau \rangle$ as a function of κ . In stark contrast to the small tracers ($\sigma_{tr} = 4$), the mean trapped time of larger tracers depends on κ significantly. Notably,

for the range of Pe explored, $\langle \tau \rangle$ increases exponentially with the bending stiffness κ . In the plot, the dashed line depicts the best exponential fit to the simulation data. The stiffness-induced increase in $\langle \tau \rangle$ is in line with the κ -dependent tendency in MSD and NGP (Figs. 3a and 3d). The slope of the exponential growth tends to decrease as the activeness of the tracer is larger. In the limit of very large Pe , AOUPs can jump to other meshes very easily even in a stiff polymer network in which the mean trapped time does not depend on κ . Apart from the mean trapped time, we also examine the distribution of trapped times at $Pe = 0, 12$, and 72 (Fig. S6). As in the case of a flexible polymer network [58], the distributions are always exponentially decaying ones regardless of the bending stiffness. Here, the effect of the bending stiffness enters in the characteristic time of the distribution, i.e., $\langle \tau \rangle$.

In Fig. 3h, we show $\langle l^2 \rangle$ as a function of κ . As expected, the flight length becomes larger with increasing Pe for all κ values investigated. By contrast, the κ -dependence in $\langle l^2 \rangle$ is nontrivial. For small Pe of $\lesssim 18$, the flight length is almost independent of κ . In this regime, the mesh-induced trapping force dominates over the active force, so hopping events are restricted to the nearest-neighbor jump only. For larger Pe of $\gtrsim 54$, the active tracer can escape from trapping and jump over multiple mesh distances. This is indeed shown in the flight length distribution plotted in Fig. S7. In this case, the hopping active tracer tends to feel increasing polymer friction as the network is stiffer, so $\langle l^2 \rangle$ decreases with κ . Notably, beyond a certain bending stiffness, the tracer effectively sees a very similar polymer environment against increasing κ , thus exhibiting a plateau in $\langle l^2 \rangle$.

In Fig. 3i, we show the long-time diffusivity D_L as a function of κ for different Pe . For small Pe , D_L is a decreasing function of κ , while for large Pe it becomes nearly independent of κ due to the excessively high activeness. We can quantitatively explain the behavior of D_L using the following relation [58]

$$D_L = \frac{1}{6} \frac{\langle l^2 \rangle}{\langle \tau \rangle + \langle \tau_{fl} \rangle}, \quad (12)$$

depicted by the solid lines in Fig. 3i. As κ increases, the flight length tends to decrease (Fig. 3h) while the trapped time increases (Fig. 3g). In addition, the mean flight time $\langle \tau_{fl} \rangle$ is found to be a decreasing function of κ (Fig. A3a). Interestingly, at large Pe values, the magnitude of $\langle \tau_{fl} \rangle$ becomes comparable with that of $\langle \tau \rangle$ and their variation tendency is opposite against increasing κ . Consequently, $\langle \tau \rangle$ and $\langle \tau_{fl} \rangle$ offset each other and the denominator in Eq. (12) becomes nearly independent of κ , resulting in a decreasing D_L with κ mainly due to $\langle l^2 \rangle$.

C. AOUPs with $\sigma_{tr} = 6$

Lastly, we study the case where the AOUP tracer size is slightly larger than the network mesh size ($\sigma_{tr} = 6 \gtrsim l_0 = 5$), as shown in Fig. 1a.

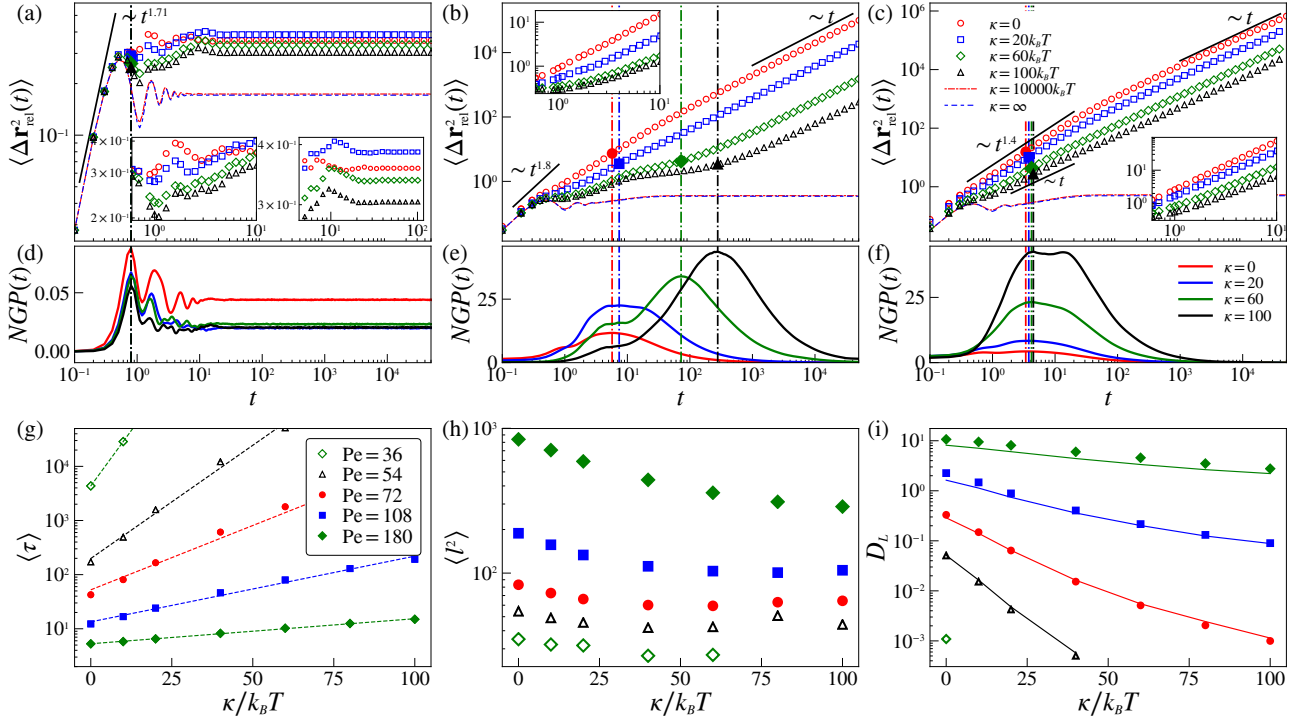


FIG. 4. MSD of tracers of size $\sigma_{\text{tr}} = 6$ for (a) $\text{Pe} = 0$, (b) $\text{Pe} = 72$, and (c) $\text{Pe} = 108$. NGP for (d) $\text{Pe} = 0$, (e) $\text{Pe} = 72$, and (f) $\text{Pe} = 108$. (g) Mean trapped time $\langle \tau \rangle$, (h) mean-square flight length $\langle l^2 \rangle$, and (i) long-time diffusivity D_L , as a function of κ , respectively. Solid lines in (i) depict D_L in Eq. (12).

Figure 4a depicts the MSD of passive tracers ($\text{Pe} = 0$) for different κ . In contrast to the previous case ($\sigma_{\text{tr}} = 5$), the short-time MSD (in $t < 1$) is found to be independent of the bending stiffness. This is because the accessible volume for the large tracer is very small regardless of the magnitude of bending stiffness κ . However, at longer times of $1 < t < 10$, the tracers are in contact with the polymers, exhibiting MSD decreasing as κ increases (Fig. 4a, left inset), similarly found in the previous case of $\sigma_{\text{tr}} = 5$. For $t > 10$, MSD increases with κ up to $\kappa = 20 k_B T$, beyond which it decreases (Fig. 4a, right inset).

Similarly to the tracer of $\sigma_{\text{tr}} = 5$, the observed bounce-back dynamics from the oscillatory behavior of the short-time MSD is pronounced in stiffer networks. As aforementioned, the observed oscillatory behavior is the consequence of the underdamped AOUP dynamics in a confining mesh. The bounce-back effect is found to be absent in the overdamped dynamics simulation of AOUPs in the same polymer network (Fig. S8).

When AOUPs have a sufficiently high self-propulsive force ($\text{Pe} = 72$), as shown in Fig. 4b, the hopping process starts to occur in $10 \lesssim t \lesssim 100$. At this activeness regime, three distinctive dynamics are observed: The tracer dynamics is ballistic in $t \lesssim \tau_0$ and Fickian in $t \gtrsim \langle \tau \rangle$. In the intermediate time ($\tau_0 \lesssim t \lesssim \langle \tau \rangle$), the tracer is subject to the viscoelastic feedback by the confining mesh. This results in intriguing MSD profiles, which illustrate intricate κ -dependent dynamics arising from the competition between the mechanical trapping force from the network and

the self-propulsive force from the tracer. The inset (Fig. 4b) shows the short-time MSD. The amplitude of MSDs tends to decrease with κ .

Figure 4c shows MSDs of the tracers at an extremely large Pe value ($\text{Pe} = 108$) in which the hopping processes become dominant. Similarly found in Fig. 3c, MSDs show superdiffusive-to-Fickian crossover dynamics at around the directional persistent time $\tau_A = 10$. In the intermediate time, the amplitude of MSDs decreases and the exponent $\alpha(t)$ is lowered to unity as κ increases.

Below the MSD plots, in Figs. 4d-f, we show NGPs in the same time axes. (See also the van-Hove self-correlation functions in Fig. S9). Figure 4d is for the passive tracer where no hopping events occur. We find the NGPs to oscillate in the short time, which reflects the bounce-back dynamics in the MSD. Overall, the magnitude of NGPs is small ($\sim 10^{-2}$), suggesting that the potential of mean force is expected to be a harmonic function (Fig. A2b). Figure 4e shows the NGPs for AOUPs with $\text{Pe} = 72$. We find that the NGP has a broad peak, particularly with a shoulder for large κ . Similarly found in Fig. 3e, the peak time and value of the NGP increase with κ . For $\text{Pe} = 108$ (Fig. 4f), the peak time of the NGP becomes less κ -dependent. However, its magnitude increases with increasing κ due to the responsive network. Such a tendency of NGP is similarly found in Fig. 3f, but the magnitude of NGP is larger by a factor of 10 when $\sigma_{\text{tr}} = 6$, signifying a huge difference in the tracer's dynamics between $\sigma_{\text{tr}} = 5$ and $\sigma_{\text{tr}} = 6$.

Figure 4g depicts the mean trapped time of AOUPs as a

function of κ for different Pe. Similarly to the case of $\sigma_{\text{tr}} = 5$, the mean trapped time becomes shorter by larger activity. Additionally, the mean trapped time increases exponentially with κ . From this relation, it can be deduced that $\ln\langle\tau\rangle \sim \kappa/(k_B T)$ in which κ predominantly modulates an energy barrier for hopping into the nearest mesh. We also confirm that the trapped time is exponentially distributed (Fig. S10), as the tracer of $\sigma_{\text{tr}} = 5$ shows. In the following section, we shall explain the observed exponential law for the mean trapped time using a first-passage time theory of AOUPs.

Figure 4h illustrates the mean-square flight length $\langle l^2 \rangle$ as a function of κ for $\text{Pe} \geq 36$. As observed in the results of $\sigma_{\text{tr}} = 5$, $\langle l^2 \rangle$ is nearly independent of κ for small Pe values. On the other hand, for large Pe values of > 108 , multiple-mesh-hopping events freely occur (Fig. S11) in which the hopping distance is on average shorter as the polymeric friction increases with the bending stiffness.

Finally, in Fig. 4i, we show the long-time diffusivity as a function of κ for different Pe. The simulation results (symbols) and the theoretical prediction [Eq. (12)] depicted by the solid lines are compared, showing a good agreement (The mean flight times $\langle\tau_{\text{fl}}\rangle$ in Fig. A3b). When Pe is small ($\text{Pe} = 54$), $\langle\tau\rangle$ dominates over $\langle\tau_{\text{fl}}\rangle$ and $\langle l^2 \rangle$ is independent of κ , resulting in an exponentially decaying D_L . For large Pe, the exponential tendency is disrupted because κ -dependent $\langle l^2 \rangle$ and $\langle\tau_{\text{fl}}\rangle$ come into play.

D. Active escape dynamics

The above trapped-and-hopping diffusion can be conceptualized as an escaping process of AOUPs from a confining potential and hopping to the nearest mesh. In this context, we explain the mean trapped times $\langle\tau\rangle$ in terms of a barrier-crossing time (τ_e) of a diffusing particle within a confining potential. As supported by the potential of mean force (Fig. A2), we approximate the confining potential as a harmonic potential within a minimal model framework. We then calculate the mean-first passage time of an AOUP under two absorbing boundaries located at the mesh boundary. From this perspective, we present the analysis of active escape dynamics from the analogy of harmonic potential, as depicted in Fig. 5a.

The overdamped AOUP dynamics in a 1-D harmonic potential $V_{\text{eff}}(x) = \frac{1}{2}kx^2$ is described by the following Langevin equation

$$\gamma \frac{dx(t)}{dt} = -kx(t) + \xi_{\text{th}}(t) + F_A(t) \quad (13)$$

and, equivalently, by the two-variable (x and F_A) Fokker-Planck equation

$$\frac{\partial p}{\partial t} = \frac{1}{\gamma} \frac{\partial}{\partial x} [kx - F_A] p + \frac{k_B T}{\gamma} \frac{\partial^2 p}{\partial x^2} + \frac{1}{\tau_A} \frac{\partial}{\partial F_A} [F_A p] + \frac{\gamma^2 v_p^2}{\tau_A} \frac{\partial^2 p}{\partial F_A^2}. \quad (14)$$

Here, $p(x, F_A, t)$ is the probability density that the position and the active force of the AOUP are found to be x and F_A

at time t , respectively. Because ξ_{th} and F_A are both Gaussian noises, the stationary distribution for the above Fokker-Planck equation is given by a bivariate Gaussian distribution, i.e., $p_{\text{st}}(x, F_A) \sim \exp[-\frac{1}{2}(x, F_A)\Sigma^{-1}(x, F_A)^T]$ where Σ is the covariance matrix. From this, we obtain the expression for the steady-state distribution of the position

$$p_{\text{st}}(x) \sim \exp\left(-\frac{\frac{1}{2}kx^2}{k_B T + \frac{\gamma^2 \tau_A v_p^2}{k\tau_A + \gamma}}\right) = \exp\left(-\frac{\frac{1}{2}kx^2}{k_B T_{\text{eff}}}\right). \quad (15)$$

The last expression allows us to introduce the effective temperature of an AOUP

$$k_B T_{\text{eff}} = k_B T + \frac{(k_B T)^2 \tau_A}{\sigma_{\text{tr}}^2 (k\tau_A + \gamma)} \text{Pe}^2, \quad (16)$$

consistent with the expression in Ref. [67]. Equation (15) suggests that the AOUP's asymptotic long-time confinement dynamics can be mapped onto that of a Brownian particle in a harmonic potential at $T = T_{\text{eff}}$. Our analytic calculation shows that the barrier-crossing time τ_e of an AOUP in the harmonic potential $V_{\text{eff}}(x)$ is the Kramers time with the effective temperature:

$$\tau_e \sim \exp\left(\frac{V}{k_B T_{\text{eff}}}\right) = \exp\left(\frac{V}{k_B T \left(1 + \frac{k_B T \tau_A}{\sigma_{\text{tr}}^2 (k\tau_A + \gamma)} \text{Pe}^2\right)}\right) \quad (17)$$

where V is the potential barrier height at the absorbing boundaries (Fig. 5a). The above expression advances the result in Ref. [68] in that it explicitly contains the role of the ambient heat bath (T).

In our framework, the details of the effective potential V are modulated by the system's physical properties, such as the bending stiffness and the mesh-to-particle size ratio. For a small bending regime, the effective potential can be reasonably approximated to

$$V \simeq V_0 + V_1 \frac{\kappa}{k_B T} \quad (18)$$

where V_0 is the potential for a flexible polymer network and the next term is responsible for the potential increase when the polymer network gains stiffness with a bending modulus κ . Combining Eqs. (17) and (18), we obtain the barrier-crossing time τ_e as follows:

$$\tau_e = \tau_e^{(\text{fl})} \exp\left(\frac{V_1}{k_B T \left(1 + \frac{\tau_A k_B T}{\sigma_{\text{tr}}^2 (k\tau_A + \gamma)} \text{Pe}^2\right)} \frac{\kappa}{k_B T}\right) \quad (19)$$

where $\tau_e^{(\text{fl})}$ is the mean escape time in the limit of a flexible polymer network ($\kappa \rightarrow 0$). Note that Eq. (19) includes two undetermined potential constants of a given polymer network: V_1 and the spring constant k , which depend on some physical parameters, e.g., the mesh-to-particle size ratio. Because both constants are independent of κ , we anticipate that the mean escape (i.e., trapped) time of an AOUP in

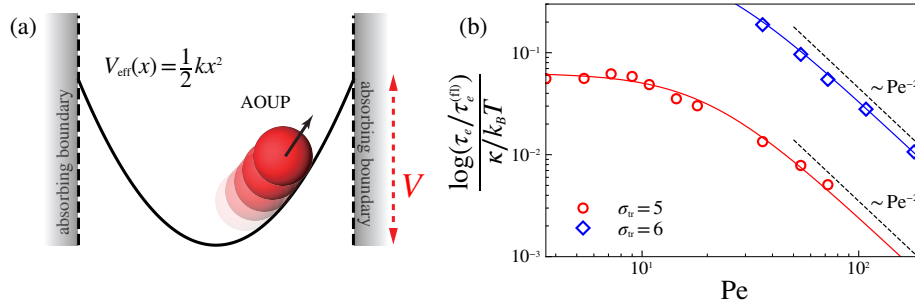


FIG. 5. (a) Illustration of AOUPs in a harmonic potential. When AOUPs cross the barrier of height V , it is considered hopping into the nearest mesh. (b) The plot of the rescaled mean trapped time, $\frac{\log(\tau_e/\tau_e^{(fl)})}{\kappa/k_B T}$, as a function of Pe . The symbols are from our simulation data and the solid lines are from Eq. (21). For $\sigma_{tr} = 5$ (red line), the fitting parameters are $V_1 = 0.063 k_B T$ and $k = 15.55 k_B T/\sigma_0^2$. For $\sigma_{tr} = 6$ (blue line), the fitting parameters are $V_1 = 0.84 k_B T$ and $k = 11.19 k_B T/\sigma_0^2$.

a polymer network follows an exponential law of the form:

$$\tau_e = \tau_e^{(fl)} \exp\left(C \frac{\kappa}{k_B T}\right) \quad (20)$$

where the prefactor $C = C(Pe, \sigma_{tr})$ reads

$$C(Pe, \sigma_{tr}) = \frac{\log(\tau_e/\tau_e^{(fl)})}{\kappa/k_B T} = \frac{V_1}{k_B T \left(1 + \frac{k_B T \tau_A}{\sigma_{tr}^2 (k \tau_A + \gamma)} Pe^2\right)} \quad (21)$$

explaining the stiffness effects on the active escaping dynamics. Our theory, Eq. (20), describes the exponential growth law of the mean trapped times of AOUPs observed in our simulation (Figs. 3g and 4g).

We obtain two important properties of the active escaping process from Eq. (19). First, the effect of bending stiffness, $C(Pe, \sigma_{tr})$, illustrates different behaviors on small and large Pe regimes. When Pe is small, the active escaping dynamics barely depends on the network stiffness (i.e., $C \simeq \frac{V_1}{k_B T}$). However, when Pe is increased, the stiffness factor C decays as $C \sim Pe^{-2}$ with Pe . In Fig. 5b, we plot the mean trapped time in the form of $\frac{\log(\tau_e/\tau_e^{(fl)})}{\kappa/k_B T}$ as a function of Pe from our simulation data, along with Eq. (21) [solid line]. When $\sigma_{tr} = 5$, the theoretical line is plotted with V_1 determined from the Brownian case ($Pe = 0$) in Fig. 3g and k being a fitting parameter. When $\sigma_{tr} = 6$, since a hopping event is rarely observed during our simulation time, we fit the data with Eq. (21), with V_1 and k being the fitting parameters. Our simulation results in Fig. 5b indeed demonstrate that the stiffness factor C illustrates the theoretically expected two scaling behaviors.

The parameter $V_1(\sigma_{tr})$ quantifies the slope of potential increase as the polymer network stiffens. Our above analysis reveals that $V_1(\sigma_{tr} = 5) = 0.063 k_B T$ and $V_1(\sigma_{tr} = 6) = 0.84 k_B T$. Note that $V_1(\sigma_{tr} = 6) \gg V_1(\sigma_{tr} = 5)$, reflecting that the effect of polymer stiffness on the active escape dynamics is dramatically amplified as a tracer is larger. Moreover, as Fig. 5b shows, the stiffness effect is larger than an order of magnitude for the tracer size of $\sigma_{tr} = 6$ than $\sigma_{tr} = 5$. This

also confirms that the stiffness effect on the active escape is dramatically increased when the tracer size increases.

IV. DISCUSSION

We studied the diffusion dynamics of active tracer particles in a semi-flexible polymer network by performing underdamped Langevin dynamics simulations. The observed tracer dynamics spans a wide time scale, ranging from the short-time ballistic dynamics to the long-time diffusive dynamics. For mesh-sized tracers that are tightly trapped in the network, we observed the bounce-back dynamics in the short-time regime [60, 65, 69], manifested by oscillations in MSDs and NGPs (Figs. 3 and 4). This unique behavior was further validated in Figs. S4 and S8, where the overdamped Langevin dynamics simulations of the same system produced the MSD without the bounce-back oscillations.

In our study, we adopted the AOUP model for the active tracer. As described in Introduction, there exist other relevant active particle models, including the active Brownian particle (ABP) model [70] or the run-and-tumble particle model [10]. In these models, the active force is consistently characterized by an exponentially decaying directional memory [71, 72], but their microscopic mechanism is distinct: The ABP moves with a constant propulsion speed while its orientation randomly changes. The run-and-tumble particle follows straight paths with intermittent tumbling events, reflecting a distinct succession of straight-line segments. It remains an open question to systematically examine how the active diffusion in a polymer network depends on these active tracer models.

To obtain an insight into the dependence of active tracer models on the active diffusion reported in Sec. III, we repeated the underdamped Langevin dynamics simulations of our semi-flexible polymer networks with the ABP model. For a direct comparison with our AOUP model, we neglected the rotational inertia and set the rotational diffusivity to $D_R = 1/(2\tau_A)$, which yields the same propulsion memory and MSDs of the AOUP described in Eqs. (4) and (5), re-

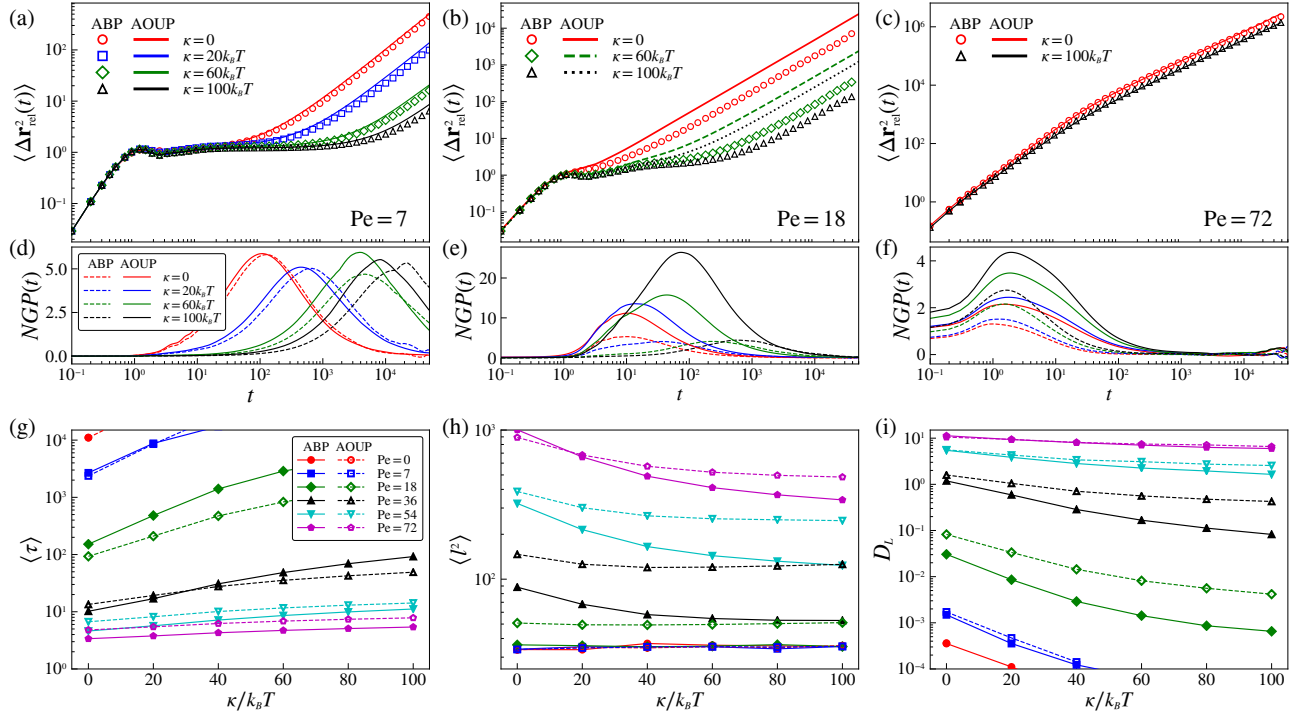


FIG. 6. The simulation results for ABP tracers ($\sigma_{\text{tr}} = 5$) in semi-flexible polymer networks in comparison with those of AOUPs of the same size (Fig. 3). MSD for (a) $Pe = 7$, (b) $Pe = 18$, and (c) $Pe = 72$. NGP for (d) $Pe = 7$, (e) $Pe = 18$, and (f) $Pe = 72$. (g) Mean trapped time $\langle \tau \rangle$, (h) mean-square flight length $\langle l^2 \rangle$, and (i) long-time diffusivity D_L as a function of κ , respectively.

spectively.

In Fig. 6a, we compare the MSDs of ABPs and AOUPs at $Pe = 7$. When Pe is relatively small compared to the potential barrier to escape from the trapping, the effect of self-propulsive movement is negligible and the MSDs for both ABP and AOUP tracers are almost identical. However, as the activeness is increased to $Pe = 18$ (Fig. 6b), we can observe the difference between the two models. Here, the microscopic features of each model play a distinct role in the MSDs. While the MSDs of the two models coincide in the short-time regime where the tracer rarely interacts with the polymer network, the AOUPs in the intermediate-to-long-time regimes consistently display larger MSDs compared to ABPs. This indicates that AOUPs have a greater propensity to escape from trapping than ABPs. Notably, when the activeness is further increased to $Pe = 72$ (Fig. 6c), the MSDs of both models converge, reflecting a scenario where trapping occurrences are rare, and ABPs and AOUPs explore the network with a similar self-propulsion tendency. In Figs. 6d-f, we analyze the NGPs. Consistent with the MSDs, non-Gaussianity of the active movement is alike for both models at $Pe = 7$ while the AOUP exhibits stronger non-Gaussian diffusion than the ABP at high Pe numbers. In Fig. 6g, we investigate the mean trapped times ($\langle \tau \rangle$) for both models. The $\langle \tau \rangle$ is similar to each other at $Pe = 7$. For intermediate Pe values, the AOUP has a shorter mean trapped time than the ABP. When Pe is increased further, the trapping effect is more negligible, resulting in a smaller difference in $\langle \tau \rangle$ between the two models. For all Pe values explored, $\langle \tau \rangle$

of the ABP is shown to increase with κ , mirroring the behavior observed in the AOUP. Figure 6h shows the mean square flight lengths of ABPs and AOUPs. The $\langle l^2 \rangle$ of AOUPs is larger than that of ABPs at intermediate Pe values, with the disparity becoming less dominant for larger Pe . Finally, Fig. 6i presents the long-time diffusivity of ABPs and AOUPs. Consistent with other observables, the difference between ABPs and AOUPs is noticeable in the regime of intermediate Pe and becomes negligible at small and large Pe values. In a nutshell, ABPs exhibit qualitatively similar trapped-and-hopping active diffusion as AOUPs, as observed in our main study. The distinction in their active diffusion is evident primarily in the intermediate Pe regime, where the active escaping dynamics from a trapped site are largely dominated by the microscopic self-propulsion mechanism inherent to each model.

V. CONCLUSIONS

We have simulated AOUPs in a semi-flexible polymer network and systematically investigated the effects of bending stiffness on the trapped-and-hopping active diffusion. We have found that the diffusivity of AOUPs is mainly governed by the particle-to-mesh size ratio and semi-flexibility of the polymer network as well as Pe .

When the tracer size is marginally smaller than the mesh size, the polymer's stiffness does not drastically affect the trapped-and-hopping dynamics. This is because the trap-

ping force is negligibly small while hopping frequently occurs in the presence of minor obstacle effects from the network. However, when the tracer size is comparable to the mesh size, the stiff polymer network hinders the hopping and enhances the trapped time. Consequently, the mean trapped time becomes longer as the polymer becomes stiffer. However, the flight length is a decreasing function of the bending stiffness only for large Pe , in which the long-jump events are more hindered by the stiff polymers. For active tracers marginally larger than the mesh size, we have observed that the tracers suffer confined motions easily when the activeness is weak. When the activeness increases, the hopping process starts to occur, by which the trapped time depends on the polymer stiffness sensitively while the flight length does not. However, for largely activated tracers, the hopping dynamics becomes dominant and the flight length changes sensitively with varying bending stiffness, while the trapped time becomes less sensitive.

Our study, which was extended from the previous work for flexible polymer networks [58], demonstrates that the polymer's semi-flexibility plays an important role in sensitively modulating the active diffusion of the mesh-sized tracers confined in the polymer network. The observed trapped-and-hopping mechanism thus provides insights to better understand the active dynamics under confinement.

ACKNOWLEDGMENTS

This work was supported by the National Research Foundation of S. Korea via No. RS-2023-00218927. W.K.K. acknowledges the financial support from the KIAS Individual Grants (CG076002) at Korea Institute for Advanced Study. We acknowledge the Center for Advanced Computation at Korea Institute for Advanced Study for providing computing resources for this work.

APPENDIX

A. Classification of trapped-and-hopping events

To classify the tracer trapping and hopping in the trajectories, we first skeletonize the trajectories. From every relative particle positions $\mathbf{r}_{\text{rel},i}(t)$, we compute the skeletonized trajectories $\hat{x} \equiv \mathcal{F}_{\text{Bi}}[\mathcal{F}_{\text{Bi}}[x]]$, where \mathcal{F}_{Bi} is the bilateral filter [64] and x is a component of the relative trajectory. This is defined as

$$\mathcal{F}_{\text{Bi}}[x] \equiv \frac{1}{W_p} \sum_{t_i \in \Omega} x_j(t_i) f(|x_j(t_i) - x_j(t_k)|) g(|t_i - t_k|), \quad (22)$$

where $W_p = \sum_{x_i \in \Omega} f(|x_j(t_i) - x_j(t_k)|) g(|t_i - t_k|)$ is the normalization factor, f and g are the Gaussian kernels given by $f(x) = e^{-x^2/\sigma_x^2}$ and $g(t) = e^{-t^2/\sigma_t^2}$. We set $\sigma_x = 5$ and $\sigma_t = 1$. The bilateral filter's edge-preserving properties

produce skeletonized trajectories \hat{x} with noise-free trapped parts and instantaneous jumps.

Next, we identify hopping events from the filtered trajectory \hat{x} by examining our criteria $|\hat{x}(t+2t_0) - \hat{x}(t-t_0)| > l_c$, where the cutoff is $l_c = 0.6 \times l_0 = 3$. We then determine the initial and final times for the hopping by checking if the original trajectory $x(t)$ and filtered trajectory \hat{x} share the same direction in one component. Specifically, if four segments $x(t+t_0) - x(t)$, $x(t) - x(t-t_0)$, $\hat{x}(t+t_0) - \hat{x}(t)$, and $\hat{x}(t) - \hat{x}(t-t_0)$ have the same direction, and the tracer is in a hopping state at $t+t_0$ or $t-t_0$, we set the tracer to be in a hopping state at t . We iteratively apply this condition to establish the initial and final hopping times.

Since the trajectory is in 3D, we define a trapped state when the trajectory is not in a hopping state for any components. The trapped time is then defined as the duration of consecutive trapped states. To determine the flight time, we find the duration of consecutive hopping states. Finally, for the flight length, we calculate the chord length of the hopping state in 3D by using two ends of positions of the consecutive hopping interval.

B. Active diffusion of small tracers

Figure A1 represents the active diffusion of small tracers ($\sigma_{\text{tr}} = 1$) in the polymer networks. For the small tracers, the polymer network acts as a trivial obstacle to the tracers. Figure A1a is the sample trajectory of small active tracers ($Pe = 1$). Figure A1b represents the MSDs for small active tracers, where the color represents Pe and the symbols represent the different stiffness κ . The simulation results show that varying the polymer's bending stiffness does not significantly affect the diffusion dynamics of small active tracers. Figures A1c–e represent the NGPs of small active tracers. The NGPs of the small active tracers in a semi-flexible polymer network exhibit only a slight increase compared to those in a flexible polymer network.

C. The potential of mean forces for tracers of size $\sigma_{\text{tr}} = 5$ and 6

For the Brownian tracer ($Pe = 0$) confined in a polymer mesh, we calculate the potential of mean force by the following relations:

$$p(x) \sim e^{-\beta U(x)} \quad (23)$$

$$U(x) = -k_B T \ln(p(x)) + k_B T \ln(p_0)$$

Here, for convenience, we set $U(0) = 0$ by adding the second term where $p_0 \equiv p(x=0)$.

Figure A2 depicts the potential of mean force calculated from the trajectories of the Brownian tracers, which shows how the potential of mean force is modulated by the polymer's stiffness.

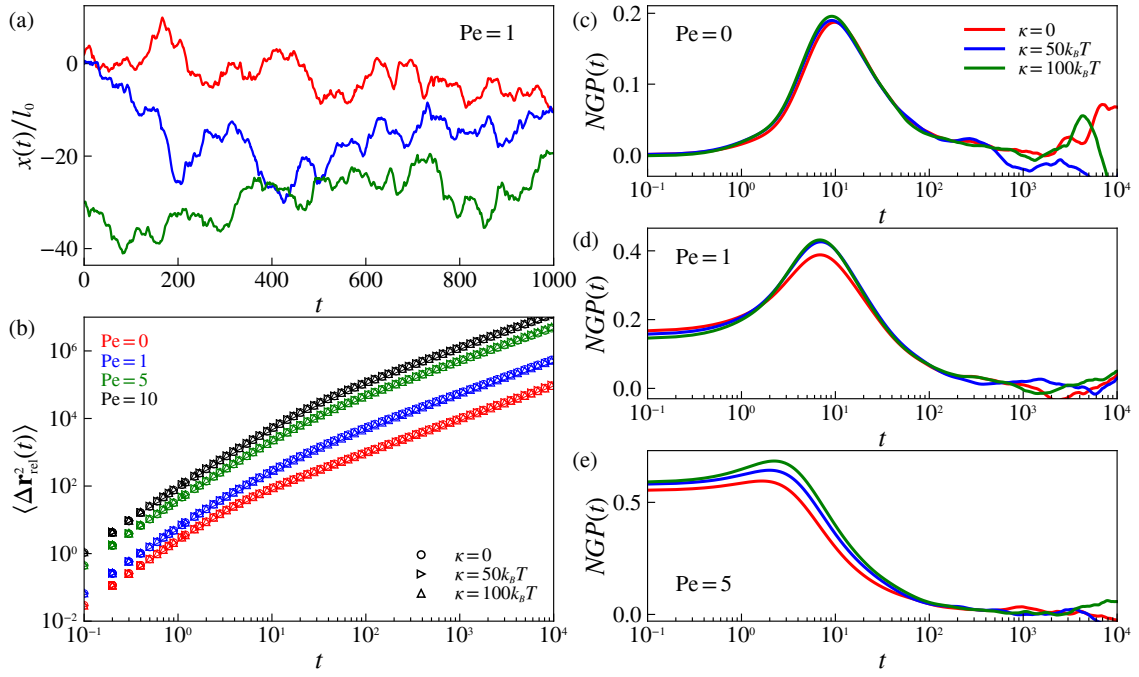


FIG. A1. Active diffusion for small active tracers. (a) Sample trajectory for different polymer network stiffness. (b) MSD (c) NGP for passive tracers (d,e) NGP for active ($Pe = 1, 5$) tracers

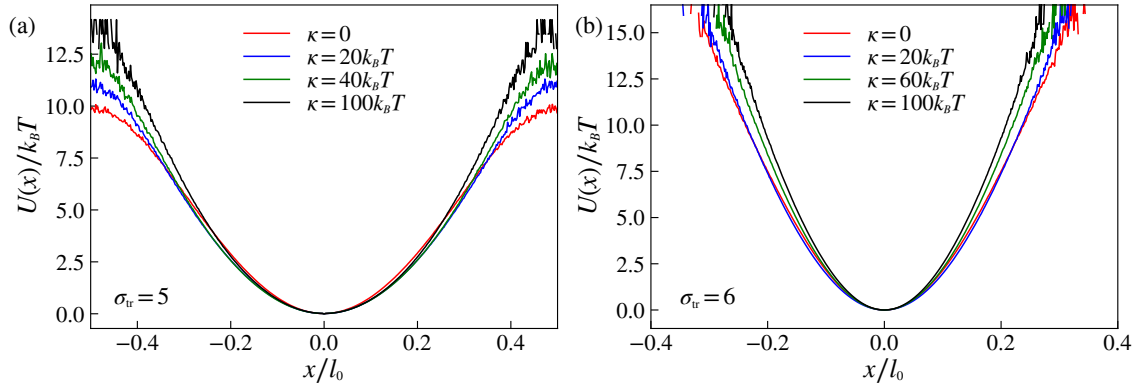


FIG. A2. The potential of mean forces for the tracers ($Pe = 0$) of size (a) $\sigma_{tr} = 5$ and (b) $\sigma_{tr} = 6$ in a flexible and semi-flexible polymer networks of $\kappa = 0, 20k_B T, 60k_B T,$ and $100k_B T$.

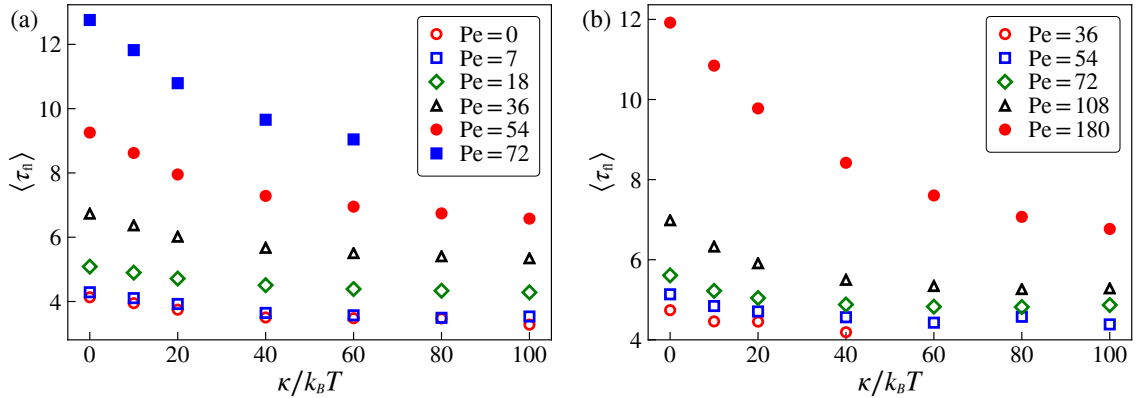


FIG. A3. Mean flight time (τ_f) of AOUPs of size (a) $\sigma_{tr} = 5$ and (b) $\sigma_{tr} = 6$ as a function of κ for various Pe values.

D. The mean flight times for tracers of size $\sigma_{tr} = 5$ and 6

Figure A3 shows the mean flight time as a function of κ for the active tracers with various Pe values.

-
- [1] L. Duarte, A. Teixeira, and L. Rizzi, Microrheology of semiflexible filament solutions based on relaxation simulations, *Soft Matter* **17**, 2920 (2021).
- [2] A. J. Engler, S. Sen, H. L. Sweeney, and D. E. Discher, Matrix elasticity directs stem cell lineage specification, *Cell* **126**, 677 (2006).
- [3] W. K. Kim, A. Moncho-Jordá, R. Roa, M. Kanduč, and J. Dzubella, Cosolute partitioning in polymer networks: Effects of flexibility and volume transitions, *Macromolecules* **50**, 6227 (2017).
- [4] C. Wagner, K. Wheeler, and K. Ribbeck, Mucins and their role in shaping the functions of mucus barriers, *Annu. Rev. Cell Dev. Biol.* **34**, 189 (2018).
- [5] A. Pathak and S. Kumar, Independent regulation of tumor cell migration by matrix stiffening and confinement, *Proc. Natl. Acad. Sci. U.S.A.* **109**, 10334 (2012).
- [6] S. Ramaswamy, Active matter, *J. Stat. Mech: Theory Exp.* **2017**, 054002 (2017).
- [7] F. Schweitzer and J. D. Farmer, *Brownian Agents and Active Particles: Collective Dynamics in the Natural and Social Sciences*, Vol. 1 (Springer, 2003).
- [8] C. Bechinger, R. Di Leonardo, H. Löwen, C. Reichhardt, G. Volpe, and G. Volpe, Active particles in complex and crowded environments, *Rev. Mod. Phys.* **88**, 045006 (2016).
- [9] M. M. Genkin, A. Sokolov, O. D. Lavrentovich, and I. S. Aranson, Topological defects in a living nematic ensnare swimming bacteria, *Phys. Rev. X* **7**, 011029 (2017).
- [10] H. C. Berg, *E. Coli in Motion* (Springer, 2004).
- [11] T. Bhattacharjee and S. S. Datta, Confinement and activity regulate bacterial motion in porous media, *Soft Matter* **15**, 9920 (2019).
- [12] J. Elgeti, R. G. Winkler, and G. Gompper, Physics of microswimmers—single particle motion and collective behavior: A review, *Rep. Prog. Phys.* **78**, 056601 (2015).
- [13] S. Ramaswamy, The mechanics and statistics of active matter, *Annu. Rev. Condens. Matter Phys.* **1**, 323 (2010).
- [14] M. C. Marchetti, J.-E. Joanny, S. Ramaswamy, T. B. Liverpool, J. Prost, M. Rao, and R. A. Simha, Hydrodynamics of soft active matter, *Rev. Mod. Phys.* **85**, 1143 (2013).
- [15] J. Tailleur and M. Cates, Sedimentation, trapping, and rectification of dilute bacteria, *Europhys. Lett.* **86**, 60002 (2009).
- [16] A. Pototsky and H. Stark, Active brownian particles in two-dimensional traps, *Europhys. Lett.* **98**, 50004 (2012).
- [17] C. Maggi, M. Paoluzzi, N. Pellicciotta, A. Lepore, L. Angelani, and R. Di Leonardo, Generalized energy equipartition in harmonic oscillators driven by active baths, *Phys. Rev. Lett.* **113**, 238303 (2014).
- [18] K. Qi, E. Westphal, G. Gompper, and R. G. Winkler, Enhanced rotational motion of spherical squirmer in polymer solutions, *Phys. Rev. Lett.* **124**, 068001 (2020).
- [19] L. Theeyancheri, R. Sahoo, P. Kumar, and R. Chakrabarti, In silico studies of active probe dynamics in crowded media, *ACS Omega* **7**, 33637 (2022).
- [20] T. Bhattacharjee and S. S. Datta, Bacterial hopping and trapping in porous media, *Nat. Commun.* **10**, 2075 (2019).
- [21] Z. Wu, Y. Chen, D. Mukasa, O. S. Pak, and W. Gao, Medical micro/nanorobots in complex media, *Chem. Soc. Rev.* **49**, 8088 (2020).
- [22] W. Wang, H. Xu, Q. Ye, F. Tao, I. Wheeldon, A. Yuan, Y. Hu, and J. Wu, Systemic immune responses to irradiated tumours via the transport of antigens to the tumour periphery by injected flagellate bacteria, *Nat. Biomed. Eng.* **6**, 44 (2022).
- [23] F. Moore, J. Russo, T. B. Liverpool, and C. P. Royall, Active brownian particles in random and porous environments, *J. Chem. Phys.* **158**, 10.1063/5.0131340 (2023).
- [24] C. Abaurrea-Velasco, C. Lozano, C. Bechinger, and J. de Graaf, Autonomously probing viscoelasticity in disordered suspensions, *Phys. Rev. Lett.* **125**, 258002 (2020).
- [25] K. S. Olsen, L. Angheluta, and E. G. Flekkøy, Active brownian particles moving through disordered landscapes, *Soft Matter* **17**, 2151 (2021).
- [26] D. Breoni, M. Schmiedeberg, and H. Löwen, Active brownian and inertial particles in disordered environments: Short-time expansion of the mean-square displacement, *Phys. Rev. E* **102**, 062604 (2020).
- [27] M. R. Shaebani, Z. Sadjadi, I. M. Sokolov, H. Rieger, and L. Santen, Anomalous diffusion of self-propelled particles in directed random environments, *Phys. Rev. E* **90**, 030701 (2014).
- [28] P. Rizkallah, A. Sarracino, O. Bénichou, and P. Illien, Microscopic theory for the diffusion of an active particle in a crowded environment, *Phys. Rev. Lett.* **128**, 038001 (2022).
- [29] L. J. Perez, T. Bhattacharjee, S. S. Datta, R. Parashar, and N. L. Sund, Impact of confined geometries on hopping and trapping of motile bacteria in porous media, *Phys. Rev. E* **103**, 012611 (2021).
- [30] M. Brun-Cosme-Bruny, E. Bertin, B. Coasne, P. Peyla, and S. Rafaï, Effective diffusivity of microswimmers in a crowded environment, *J. Chem. Phys.* **150**, 10.1063/1.5081507 (2019).
- [31] O. Chepizhko and F. Peruani, Diffusion, subdiffusion, and trapping of active particles in heterogeneous media, *Phys. Rev. Lett.* **111**, 160604 (2013).
- [32] A. Dehkharghani, N. Waisbord, and J. S. Guasto, Self-transport of swimming bacteria is impaired by porous microstructure, *Commun. Phys.* **6**, 18 (2023).
- [33] M.-B. Luo and D.-Y. Hua, Simulation study on the mechanism of intermediate subdiffusion of diffusive particles in crowded systems, *ACS omega* **8**, 34188 (2023).
- [34] P. Chopra, D. Quint, A. Gopinathan, and B. Liu, Geometric effects induce anomalous size-dependent active transport in structured environments, *Phys. Rev. Fluids* **7**, L071101 (2022).
- [35] X.-Z. Cao, H. Merlitz, C.-X. Wu, and M. G. Forest, Chain stiffness boosts active nanoparticle transport in polymer networks, *Phys. Rev. E* **103**, 052501 (2021).
- [36] P. Kumar and R. Chakrabarti, Dynamics of self-propelled tracer particles inside a polymer network, *Phys. Chem. Chem. Phys.* 10.1039/D2CP04253C (2023).
- [37] A. Godec, M. Bauer, and R. Metzler, Collective dynamics effect transient subdiffusion of inert tracers in flexible gel networks, *New J. Phys.* **16**, 092002 (2014).

- [38] H. Zhou and S. B. Chen, Brownian dynamics simulation of tracer diffusion in a cross-linked network, *Phys. Rev. E* **79**, 021801 (2009).
- [39] P. Kumar, L. Theeyancheri, S. Chaki, and R. Chakrabarti, Transport of probe particles in a polymer network: Effects of probe size, network rigidity and probe-polymer interaction, *Soft Matter* **15**, 8992 (2019).
- [40] P. Licinio and A. Teixeira, Anomalous diffusion of ideal polymer networks, *Phys. Rev. E* **56**, 631 (1997).
- [41] Y. Lu, X.-Y. Liu, and G.-H. Hu, Double-spring model for nanoparticle diffusion in a polymer network, *Macromolecules* **55**, 4548 (2022).
- [42] Y. Lu and G.-H. Hu, A potential barrier in the diffusion of nanoparticles in ordered polymer networks, *Soft Matter* **17**, 6374 (2021).
- [43] A. Martín-Molina and M. Quesada-Pérez, A review of coarse-grained simulations of nanogel and microgel particles, *J. Mol. Liq.* **280**, 374 (2019).
- [44] M. Quesada-Pérez, J.-A. Maroto-Centeno, M. d. M. Ramos-Tejada, and A. Martín-Molina, Coarse-grained simulations of solute diffusion in crosslinked flexible hydrogels, *Macromolecules* **55**, 1495 (2022).
- [45] B.-R. Zhao and B. Li, Molecular simulation of hopping mechanisms of nanoparticles in regular cross-linked polymer networks, *J. Chem. Phys.* **157**, 104901 (2022).
- [46] S. B. Chen, Dissipative particle dynamics simulation of nanoparticle diffusion in a crosslinked polymer network, *J. Phys. Chem. B* **126**, 7184 (2022).
- [47] H. W. Cho, H. Kim, B. J. Sung, and J. S. Kim, Tracer diffusion in tightly-meshed homogeneous polymer networks: A brownian dynamics simulation study, *Polymers* **12**, 2067 (2020).
- [48] M. Quesada-Pérez and A. Martín-Molina, Solute diffusion in gels: Thirty years of simulations, *Adv. Colloid Interface Sci.* **287**, 102320 (2021).
- [49] L.-H. Cai, S. Panyukov, and M. Rubinstein, Hopping diffusion of nanoparticles in polymer matrices, *Macromolecules* **48**, 847 (2015).
- [50] V. Sorichetti, V. Hugouvieux, and W. Kob, Dynamics of nanoparticles in polydisperse polymer networks: From free diffusion to hopping, *Macromolecules* **54**, 8575 (2021).
- [51] Z. Xu, X. Dai, X. Bu, Y. Yang, X. Zhang, X. Man, X. Zhang, M. Doi, and L.-T. Yan, Enhanced heterogeneous diffusion of nanoparticles in semiflexible networks, *ACS nano* **15**, 4608 (2021).
- [52] Y. Du, H. Jiang, and Z. Hou, Study of active brownian particle diffusion in polymer solutions, *Soft Matter* **15**, 2020 (2019).
- [53] L. Theeyancheri, S. Chaki, N. Samanta, R. Goswami, R. Chelakkot, and R. Chakrabarti, Translational and rotational dynamics of a self-propelled janus probe in crowded environments, *Soft Matter* **16**, 8482 (2020).
- [54] C. Yuan, A. Chen, B. Zhang, and N. Zhao, Activity-crowding coupling effect on the diffusion dynamics of a self-propelled particle in polymer solutions, *Phys. Chem. Chem. Phys.* **21**, 24112 (2019).
- [55] Y. Chen, R. Yan, and N. Zhao, Passive and active tracer dynamics in polymer solutions with isotropic-to-nematic phase transition, *Physical Chemistry Chemical Physics* **24**, 7415 (2022).
- [56] A. Zöttl, Dynamics of squirmers in explicitly modeled polymeric fluids, *Europhys. Lett.* 10.1209/0295-5075/acdf18 (2023).
- [57] R. Sahoo, L. Theeyancheri, and R. Chakrabarti, Transport of a self-propelled tracer through a hairy cylindrical channel: interplay of stickiness and activity, *Soft Matter* **18**, 1310 (2022).
- [58] Y. Kim, S. Joo, W. K. Kim, and J.-H. Jeon, Active diffusion of self-propelled particles in flexible polymer networks, *Macromolecules* **55**, 7136 (2022).
- [59] G. Zhang, A. Chazirakis, V. A. Harmandaris, T. Stuehn, K. C. Daoulas, and K. Kremer, Hierarchical modelling of polystyrene melts: From soft blobs to atomistic resolution, *Soft Matter* **15**, 289 (2019).
- [60] G. P. Nguyen, R. Wittmann, and H. Löwen, Active ornstein-uhlenbeck model for self-propelled particles with inertia, *J. Phys. Condens. Matter* **34**, 035101 (2021).
- [61] F. J. Sevilla, R. F. Rodríguez, and J. R. Gomez-Solano, Generalized ornstein-uhlenbeck model for active motion, *Phys. Rev. E* **100**, 032123 (2019).
- [62] W. K. Kim, M. Kanduč, R. Roa, and J. Dzubiella, Tuning the permeability of dense membranes by shaping nanoscale potentials, *Phys. Rev. Lett.* **122**, 108001 (2019).
- [63] S. Plimpton, Fast parallel algorithms for short-range molecular dynamics, *J. Comput. Phys.* **117**, 1 (1995).
- [64] C. Tomasi and R. Manduchi, Bilateral filtering for gray and color images, in *Sixth International Conference on Computer Vision (IEEE, 1998)* pp. 839–846.
- [65] L. Caprini and U. Marini Bettolo Marconi, Inertial self-propelled particles, *J. Chem. Phys.* **154**, 024902 (2021).
- [66] T. Debnath, P. Chaudhury, T. Mukherjee, D. Mondal, and P. K. Ghosh, Escape kinetics of self-propelled particles from a circular cavity, *J. Chem. Phys.* **155**, 194102 (2021).
- [67] G. Szamel, Single active particle in a harmonic potential: Question about the existence of the jarzynski relation, *Phys. Rev. E* **107**, 054602 (2023).
- [68] E. Woillez, Y. Kafri, and N. S. Gov, Active trap model, *Phys. Rev. Lett.* **124**, 118002 (2020).
- [69] H. Löwen, Inertial effects of self-propelled particles: From active brownian to active langevin motion, *J. Chem. Phys.* **152**, 10.1063/1.5134455 (2020).
- [70] J. R. Howse, R. A. Jones, A. J. Ryan, T. Gough, R. Vafabakhsh, and R. Golestanian, Self-motile colloidal particles: From directed propulsion to random walk, *Phys. Rev. Lett.* **99**, 048102 (2007).
- [71] F. Mori, P. Le Doussal, S. N. Majumdar, and G. Schehr, Condensation transition in the late-time position of a run-and-tumble particle, *Phys. Rev. E* **103**, 062134 (2021).
- [72] R. Sarkar, I. Santra, and U. Basu, Stationary states of activity-driven harmonic chains, *Phys. Rev. E* **107**, 014123 (2023).